PCCP

Accepted Manuscript

ROYAL SOCIETY OF CHEMISTRY

www.rsc.org/pccp

Physical Chemistry Chemical Physics
CREATED USING THE RSC LaTeX PCCP ARTICLE TEMPLATE – SEE www.rsc.org/electronicfiles FOR DETAILS
ARTICLE TYPE www. rsc.org/xxxxxx | XXXXXXXX

Singlet Ground State Actinide Chemistry with Geminals

Paweł Tecmer, Katharina Boguslawski and Paul W. Ayers

Received Xth XXXXXXXXXX 20XX, Accepted Xth XXXXXXXXX 20XX
First published on the web Xth XXXXXXXXXX 200X
DOI: 10.1039/b000000x

We present the first application of the variationally Orbital Optimized Antisymmetric Product of 1-reference orbital Geminals (vOO-AP1roG) method to singlet-state actinide chemistry. We assess the accuracy and reliability of the AP1roG ansatz in modelling the ground-state electronic structure of small actinide compounds by comparing it to standard quantum chemistry approaches. Our study of the ground state spectroscopic constants (bond lengths and vibrational frequencies) and potential energy curves of actinide oxides (UO_2^{2+} and ThO_2) as well as the energetic stability of ThC_2 isomers reveals that vOO-AP1roG describes the electronic structure of heavy-element compounds accurately, at mean-field computational cost.

1 Introduction

Fundamental interest in actinide compounds originates from their rich coordination chemistry, unusual bonding schemes, catalytic properties,[1–9] and importance in nuclear waste reprocessing.[10–12] Unfortunately, the acute toxicity, radioactivity, and instability of most actinide species hamper experimental studies on actinide reactivity and restrict deeper insights into actinide chemistry. Therefore, theoretical modelling of electronic structures, bonding properties, structural and spectroscopic parameters, as well as relative stabilities of actinide-containing molecules, is highly desirable. This remains, however, a difficult task, even for present-day quantum chemistry.[13,14]

To accurately describe the electronic structure of actinide species, we have to include relativistic effects and perform a correlated treatment of a large number of electrons.[15–18] Specifically, the valence atomic $5f$, $6d$, $7s$, and $6p$ orbitals participate in chemical bonding, are quasi-degenerate, and have similar spatial extent.[19] Furthermore, numerical examples reveal that the valence $5d$ orbitals have non-negligible contribution to the electron correlation energy of some actinide species.[20,21] Consequently, a reliable treatment of electron correlation effects in actinide-containing molecules usually requires a multi-reference treatment with a large active space.[22,23] Standard approaches to the strong electron correlation problem in actinide chemistry are the Complete Active Space Self-Consistent Field[24,25] (CASSCF) method, the Multi-Reference Configuration Interaction (MRCI)[26] approach and the Fock-space formulation of Coupled Cluster (CC) theory[27–29] (see Refs. 20,21,30–42 for recent applications). These methods are, however, often limited to prototypical model systems that serve as small building blocks of realistic actinide compounds that can be isolated experimentally.[43] Somewhat larger actinide molecules[44] can be modeled using tensor-network-based approaches like the Density Matrix Renormalization Group[45,46] (DMRG) algorithm. However, DMRG and similar approaches still require the introduction of an active space to be computationally feasible.

Computational studies on large realistic actinide compounds are currently dominated by Density Functional Theory[47] (DFT), which provides an efficient description of electron correlation effects.[48,49] Despite the successful results of many DFT studies supporting experimental findings in the field of actinide chemistry (see, for example, Refs. 42,50–62), DFT can yield erroneous predictions for systems that do not have a single dominant electron configuration.[21,40,63,64] This motivates the development of new computationally feasible correlated approaches for actinide chemistry. Such methods will allow us to reliably model realistic actinide species.

One promising solution to that problem can be found in geminal approaches.[65–67] Geminal-based methods use two-electron functions to model the correlated motions of electrons efficiently. Some examples for geminal-based approaches are generalized-valence-bond perfect-pairing[68–70] (GVB-PP), the antisymmetric product of strongly orthogonal geminals[71–75] (APSG), the particle-number projected Hartree–Fock–Bogoliubov ansatz,[76] the antisymmetric product of interacting geminals[76–89] (APIG), and the Antisymmetric Product of 1-reference orbital Geminal[66] (AP1roG). Recently, we have shown that AP1roG is a suitable model to describe strong electron correlation in some well-known multi-reference molecules.[67,90–92] The AP1roG ansatz can be writ-

tecmer@mcmaster.ca; ayers@mcmaster.ca
Department of Chemistry and Chemical Biology, McMaster University, Hamilton, 1280 Main Street West L8S 4M1, Canada

ten as

$$|\text{AP1roG}\rangle = \exp\left(\sum_{i=1}^{P}\sum_{a=P+1}^{K} c_i^a a_a^\dagger a_{\bar{a}}^\dagger a_{\bar{i}} a_i\right)|\Phi_0\rangle, \qquad (1)$$

where a_p, $a_{\bar{p}}$ are the electron annihilation operators for spin-up (p) and spin-down electrons ($\bar{p}$), $|\Phi_0\rangle$ is some independent-particle wave function (for instance the Hartree–Fock (HF) determinant), and $\{c_i^a\}$ is the geminal coefficient matrix. We should note that if we impose specific restrictions on the structure of $\{c_i^a\}$, we can deduce different geminal models.[65]

While the computational cost of AP1roG (or pair Coupled Cluster Doubles[93–95]) is comparable to DFT, AP1roG describes systems with quasi-degenerate electronic levels, transition state structures,[92] and bond breaking processes[66,90,91] accurately, provided the orbitals are optimized and the optimal solution is symmetry-broken.[67,96] We should note that due to the four-index transformation of the electron repulsion integrals, the computational scaling deteriorates to $\mathcal{O}(K^5)$.[67]

Similar to orbital optimized CC methods, there are different techniques to optimize the one-particle basis functions within the AP1roG framework.[67,91,92] Recent numerical studies showed that the variational orbital optimization (vOO-AP1roG[67]) approach is superior to approximate non-variational techniques and represents the most robust and reliable orbital optimization scheme for AP1roG.[91,92] Throughout this paper we will abbreviate vOO-AP1roG simply as AP1roG. In this optimization scheme, the orbitals are chosen to minimize the AP1roG energy functional subject to the constraint that the AP1roG coefficient equations are satisfied. In intermediate normalization, the energy Lagrangian has the form

$$\mathscr{L} = \langle\Phi_0|e^{\boldsymbol{\kappa}}\hat{H}e^{-\boldsymbol{\kappa}}|\text{AP1roG}\rangle + \sum_{i,a}\lambda_i^a\left(\langle\Phi_{i\bar{i}}^{a\bar{a}}|e^{\boldsymbol{\kappa}}\hat{H}e^{-\boldsymbol{\kappa}}|\text{AP1roG}\rangle - Ec_i^a\right), \qquad (2)$$

where $\{\lambda_i^a\}$ are the Lagrange multipliers and $\boldsymbol{\kappa}$ denotes the orbital rotation. The requirement that the derivative of $\mathscr{L}$ with respect to the Lagrange multipliers $\{\lambda_i^a\}$ is stationary results in the standard set of equations for the geminal coefficients $\{c_i^a\}$,[67] while the stationary requirement of $\mathscr{L}$ with respect to the geminal coefficients, $\frac{\partial\mathscr{L}}{\partial c_i^a} = 0$, leads to a set of equations for the Lagrange multipliers, analogous to the Λ-equations in CC theory.[97] The variational orbital gradient is the derivative of $\mathscr{L}$ with respect to the orbital rotation coefficients $\{\kappa_{pq}\}$.[92]

We should stress that the resulting orbital optimized AP1roG wave function is size-extensive (by construction, cf. eq. (1)) and size-consistent (because of orbital optimization).[67,90,91,93,94]

Currently, the AP1roG approach is limited to closed-shell systems. While extensions to open-shell systems are possible, they are yet to be developed.[65]

In this article, we assess the accuracy and reliability of AP1roG to model singlet-state actinide chemistry focusing on small actinide model complexes that represent non-trivial multi-reference problems. The computational methodology is summarized in section 2. In section 3, we discuss spectroscopic constants (bond length and symmetric stretching vibrational frequency) and potential energy surfaces of UO_2^{2+} and ThO_2, as well as the energetic stability of the singlet-state structural isomers of ThC_2. Finally, we conclude in section 4.

2 Computational Details

2.1 Relativity and Basis Sets

Scalar relativistic effects were incorporated through relativistic effective core potentials (RECP).[98] In all calculations, we have used a small core (SC) RECP (60 electrons in the core) for heavy elements with the following contraction scheme $(12s11p10d8f) \rightarrow [8s7p6d4f]$.[99] For lighter elements (O and C), the cc-pVDZ basis set of Dunning was employed, $(10s5p1d) \rightarrow [4s3p1d]$.[100] We note that all the systems studied in this work have closed-shell electron configurations which are essentially not affected by the presence of spin–orbit coupling.

2.2 Structures and Fitting Protocol

We have used a linear structure for UO_2^{2+} and a bent structure ($\measuredangle$ (O–Th–O) = 120) for ThO_2. The three structures of singlet ground-state ThC_2 compounds are displayed in Figure 1.

The spectroscopic constants of UO_2^{2+} and ThO_2 for all wave function methods (excluding DFT) were obtained from a generalized Morse function fit.[101] Each fit was based on at least 12 single point calculations, displaced by 0.05 Å around the equilibrium distance and larger displacements at stretch geometries. The harmonic vibrational frequencies were calculated numerically using the five-point finite difference stencil.[102]

2.3 vOO-AP1roG

All geminal calculations have been performed in a developer version of the HORTON software package.[103] All restricted AP1roG calculations were allowed to freely relax without any spatial symmetry constraints, i.e., no point group symmetry was imposed. For all molecules, all orbitals were active, which results in an active space containing 115 orbitals and 46 electrons for UO_2^{2+} and ThO_2, while for ThC_2 44 electrons were correlated. The natural occupation numbers were computed from the (response) 1-particle reduced density matrix (1-RDM). Note that AP1roG is a product of natural geminals, so the 1-RDM is diagonal.

Furthermore, we analysed all eigenvalues of the exact orbital Hessian for each point on the potential energy surface of UO_2^{2+} and ThO_2 as well as for the ThC_2 isomers to ensure that all points correspond to local minima, not saddle points.[95]

The single-orbital entropy was calculated from 1-RDMs as implemented (see Ref.[104] for details) in the HORTON program package.

2.4 CASSCF

All CASSCF calculations have been performed using the MOLPRO2012 software package.[105,106]

For the UO_2^{2+} molecule, we performed CAS(10,10)SCF, CAS(12,12)SCF and CAS(12,16)SCF calculations using D_{2h} point group symmetry. Specifically, CAS(10,10)SCF comprises the $1\pi_g$, $2\pi_u$, $3\sigma_u$, $3\pi_u$, $4\sigma_u$, and $2\pi_g$ orbitals, CAS(12,12)SCF contains additional $3\sigma_g$ and $4\sigma_g$ orbitals and the CAS(12,16)SCF is further extended by inclusion of the doubly degenerate $1\phi_u$ and $1\delta_u$ orbitals.

For the ThO_2 molecule, we performed CAS(12,12)SCF calculation. Specifically, we correlated the 5σ, 2π, 3π, 6σ, 7σ, 4π, 5π and 8σ orbitals imposing C_{2v} point group symmetry.

For the ThC_2 isomers (see structures **1**, **2** and **3** in Figure 1), we performed CAS(10,14)SCF as in Ref.[107] While we imposed C_{2v} point group symmetries on **1** and **3**, compound **2** was calculated in C_s point group symmetry.

2.5 Coupled-Cluster and MP2

The second-order Møller–Plesset perturbation theory (MP2), coupled cluster doubles (CCD), CC singles and doubles (CCSD) as well as CC singles, doubles and perturbative triples (CCSD(T)) calculations have been carried out in the DALTON2013 software package.[108] In each case, all electrons and orbitals were correlated and no spatial symmetry was imposed.

2.6 DFT

The structure optimization and vibrational frequency calculations employing the PBE[109] and PBE0[110] exchange–correlation functionals were carried out in the MOLPRO2012[105,106] software package. We imposed D_{2h} and C_{2v} spatial symmetries for UO_2^{2+} and ThO_2, respectively. (The O–Th–O angle was kept frozen at 120 degrees during the optimization procedure).

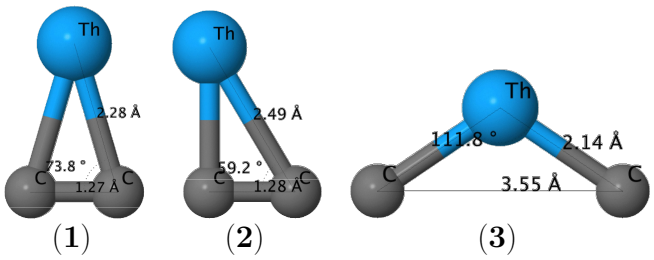

Fig. 1 Optimized singlet ground-state structures of ThC_2 (taken from Ref. 107).

3 Theoretical Modelling of Actinide Chemistry

3.1 Spectroscopic Constants and Potential Energy Surfaces of Actinide Oxides

The theoretical description of ground state spectroscopic properties of actinide oxides at the correlated level has been a subject of many scientific articles in the past decade.[35,36,58,111–115] Unfortunately, the variety of basis sets, relativistic Hamiltonians, and RECP types makes them difficult to compare. To allow for a direct assessment of the accuracy of AP1roG, we generated reference data from standard electron correlation methods.

3.1.1 Uranyl Cation. The uranyl cation (UO_2^{2+}) constitutes the most pervasive actinide oxide. This small building block is often found in larger actinide complexes and usually adopts a linear geometry. The bending tendency of the UO_2^{2+} unit is reduced by the presence of the uranium $6p$ orbitals, which are "pushed from below" by the oxygen $2s$ orbitals.[116] This leads to a strong mixing of uranium $5f$ orbitals with the highest occupied molecular orbital (HOMO).[116]

Table 1 summarizes bond lengths and vibrational frequencies of UO_2^{2+} obtained from various quantum chemistry methods. Our HF SC-RECP equilibrium bond length of 1.646 Å and vibrational frequency of 1217 cm^{-1} are in very good agreement with the all-electron four-component (4C) calculations of Dyall using the Dirac–Coulomb (DC) Hamiltonian.[117] Adding electron correlation on top of HF elongates the UO bond and lowers the symmetric vibrational frequencies (cf. Table 1). While MP2 overestimates the bond lengths and underestimate the frequencies compared to CCSD(T), the opposite is true for CCD and CCSD. CAS(12,12)SCF better matches the CCSD(T) data than CAS(10,10)SCF. The overall performance of AP1roG is satisfactory compared to standard quantum chemistry methods. As expected, the missing dynamic electron correlation energy in AP1roG results in shorter bond lengths and higher vibrational frequencies compared to MP2 and CCSD(T) or DFT. Yet, the AP1roG bond length (r_e=1.671 Å) and symmetric stretching frequency (ν_s=1141

cm^{-1}) are in excellent agreement with CCD and CCSD as well as hybrid DFT.

The advantage of AP1roG over conventional CC-based and DFT methods is its ability to dissociate multiple bonds.[67,90,91] This is also the case for UO_2^{2+}, where only CASSCF and AP1roG converged at distances larger than 2.10 Å. The resulting potential energy surfaces for the symmetric dissociation of the U-O bonds are presented in Figure 2. CAS(10,10)SCF and CAS(12,12)SCF give similar potential energy surfaces, that differ qualitatively from the CAS(12,16)SCF and AP1roG potential energy surfaces. (We should note that it was impossible to converge CAS(12,16)SCF calculations with the ϕ_u and δ_u orbitals in the active space at distances shorter than 1.800 Å). While the smaller active space calculations result in potential energy surfaces without a plateau, the inclusion of non-bonding uranium ϕ_u and δ_u orbitals in CAS(12,16)SCF gives a potential energy surface with a shoulder at 2.4 Å. The AP1roG potential energy curve features two successive shoulders at 2.00 Å and at 2.10 Å, respectively.

To better understand the bonding situation and explain the origin of the double shoulder potential energy surface in UO_2^{2+}, we performed an orbital entanglement analysis[23,104] and analysed valence orbitals and their natural occupation numbers at various distances. Figure 3 depicts all orbitals with significant values of the single-orbital entropy $s(1)_i$. $s(1)_i$ has already proven to be a powerful tool to analyse complex electronic structures[23,118] and dissect chemical bonds.[119–121] Specifically, the single orbital-entropy quantifies the entanglement of orbital i and measures the importance of an orbital in the correlated electronic wave function.[104]

At the equilibrium distance all orbitals are only weakly entangled (cf. Figure 3a), with dominant contributions of orbitals 18-29. These are the molecular orbitals that participate in bonding, i.e., linear combinations of oxygen atomic p orbitals and uranium atomic f_π and f_σ orbitals. At this U–O distance the UO_2^{2+} molecule can be well represented by a single-reference method as all the natural occupation numbers are close to 0 or 2 (see box in Figure 3a).

Table 1 Spectroscopic constants: bond lengths (r_e) and symmetric vibrational frequencies (ν_s) of UO_2^{2+} obtained from different methods.

Method		r_e [Å]	ν_s [cm^{-1}]
HF	SC-RECP (1C)	1.646	1217
	DC (4C)[117]	1.650	1234
post-HF	MP2	1.745	854
	CCD	1.687	1137
	CCSD	1.693	1090
	CCSD(T)	1.712	1031
	CAS(10,10)SCF	1.694	1085
	CAS(12,12)SCF	1.707	1034
	AP1roG	1.671	1141
DFT	PBE	1.715	1085
	PBE0	1.683	1172

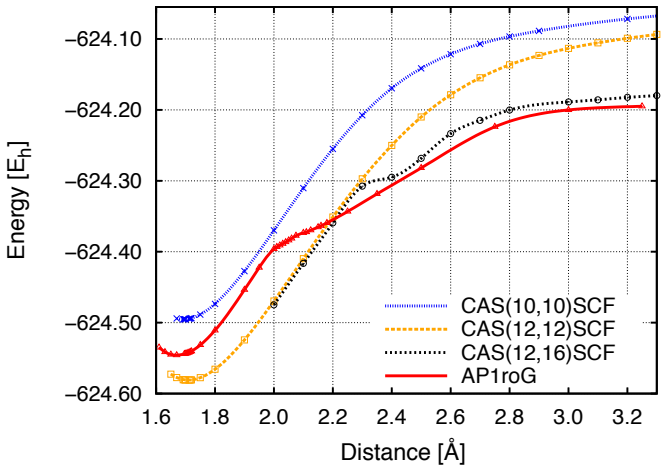

Fig. 2 AP1roG and CASSCF potential energy surfaces for the symmetric dissociation of UO_2^{2+}.

When the two oxygen atoms are pulled apart from the uranium center, orbitals 22-25 become strongly entangled. At a distance of 2.00 Å , orbitals 23 and 24 (π-type orbitals involved in bonding) have the largest value of $s(1)_i$. Molecular orbitals 22 and 25 are composed of atomic uranium f_σ and oxygen p_σ orbitals. Passing the first shoulder on the potential energy surface, at 2.01 Å (cf. Figure 2c), the electronic structure changes. From this distance onwards, the characteristic non-bonding ϕ orbitals of uranium become occupied, suggesting their importance in CASSCF calculations during the dissociation process. At 2.11 Å (the second shoulder), the 'pushing from below' mechanism breaks down and the uranium f_σ-orbital does not participate in bonding any more (cf. Figure 3e). Hence, the double-shoulder potential energy surface of UO_2^{2+} results from different bonding patterns at 2.00 Å and 2.10 Å, respectively.

Pulling the oxygen atoms further apart from the uranium center, the number of singly-occupied orbitals with large values of $s(1)_i$ gradually increases (cf. Figures 3f–3i). At 2.75 Å, there are 6 maximally entangled orbitals (21-26). These are the uranium f and oxygen p atomic orbitals. Finally, at around 3.25 Å, the U–O bonds are fully dissociated with 8 maximally entangled singly occupied orbitals. As shown in Figure 3j, AP1roG predicts uranium to have charge 2+ and the [Rn]:5f^{3}7s^1 electronic configuration in the dissociation limit.

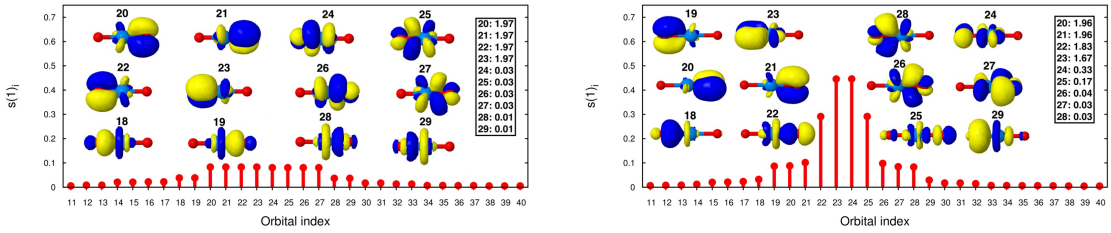

(a) $d_{\mathrm{UO}} = 1.670$ Å

(b) $d_{\mathrm{UO}} = 2.000$ Å

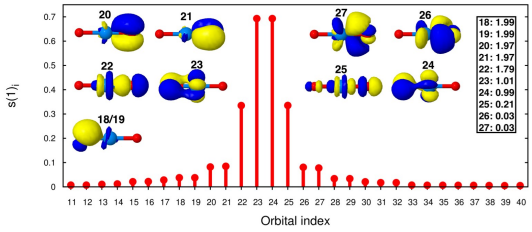

(c) $d_{\mathrm{UO}} = 2.010$ Å

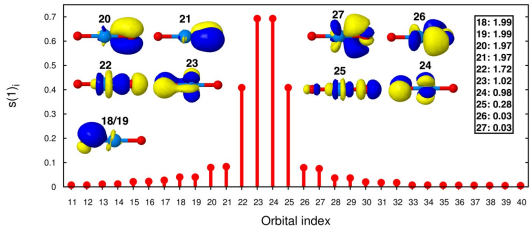

(d) $d_{\mathrm{UO}} = 2.075$ Å

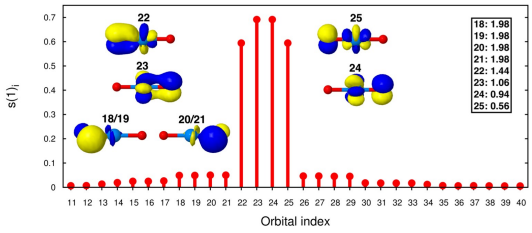

(e) $d_{\mathrm{UO}} = 2.110$ Å

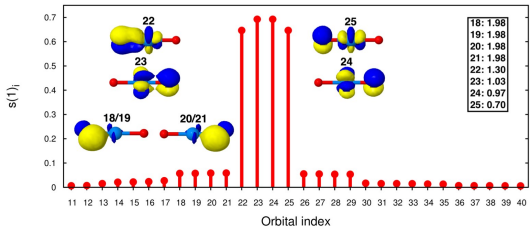

(f) $d_{\mathrm{UO}} = 2.250$ Å

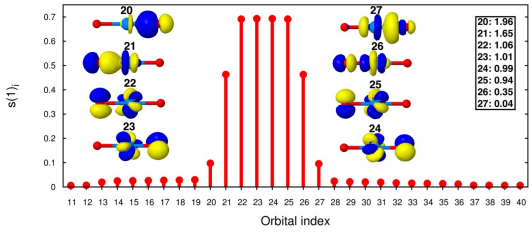

(g) $d_{\mathrm{UO}} = 2.500$ Å

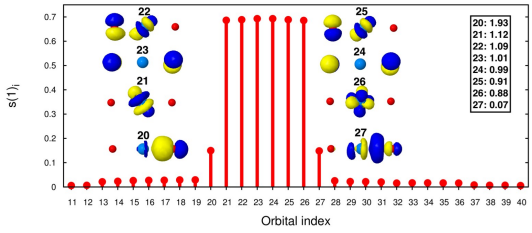

(h) $d_{\mathrm{UO}} = 2.750$ Å

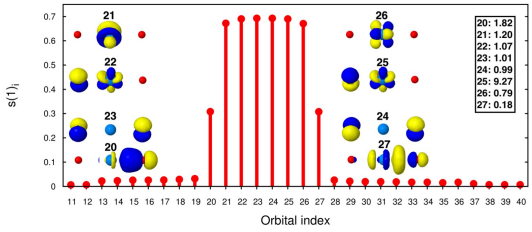

(i) $d_{\mathrm{UO}} = 3.000$ Å

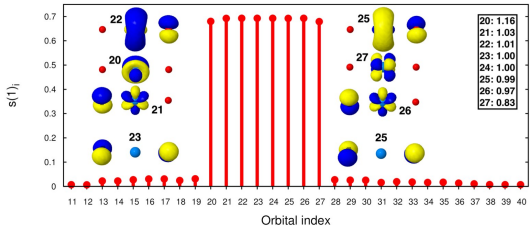

(j) $d_{\mathrm{UO}} = 3.250$ Å

Fig. 3 Comparison of AP1roG single-orbital entropies $s(1)_i$, valence orbitals, and their natural occupation numbers for the UO_2^{2+} molecule at different inter-atomic distances. $s(1)_i$ and the natural occupation numbers are determined from the response 1-RDM.

Table 2 Spectroscopic constants: bond lengths (r_e) and symmetric vibrational frequencies (ν_s) of ThO_2 ($\measuredangle$ (O–Th–O) = 120) obtained from different methods.

Method		r_e [Å]	ν_s [cm^{-1}]
HF	SC-RECP (1C)	1.895	893
	DC (4C) [117]	1.898	896
post-HF	MP2	1.938	791
	CCD	1.919	813
	CCSD	1.924	808
	CCSD(T)	1.937	808
	CAS(12,12)SCF	1.935	882
	AP1roG	1.908	909
DFT	PBE	1.906	803
	PBE0	1.890	835

3.1.2 Thorium Oxide. Although thorium oxide (ThO_2) is isoelectronic to UO_2^{2+}, its actinide-oxygen bond is completely different. The thorium atomic $6d$ orbitals lie below the $5f$ orbitals, which leads to a bent geometry of ThO_2 ($\measuredangle$ (O–Th–O) = 120) and remarkably long actinide-oxygen bond distances.[117]

Table 2 collects the spectroscopic constants for ThO_2 obtained from different approaches. Similar to UO_2^{2+}, our SC-RECP HF bond lengths and vibrational frequencies agree very well with the 4C-DC reference calculations of Dyall.[117] Again, this observation supports the right choice and good accuracy of RECP. The Th–O bond lengths and vibrational frequencies calculated form AP1roG are in good agreement with other computational methods. However, the overall accuracy of AP1roG with respect to CCSD(T) and other methods is worse than for UO_2^{2+}. Since CAS(12,12)SCF gives almost identical vibrational frequencies as AP1roG and both methods overestimate the CCSD(T) reference data by approximately 100 cm^{-1}, dynamic electron correlation effects are more important at the equilibrium bond lengths in ThO_2 than in UO_2^{2+}.

The AP1roG and CAS(12,12)SCF symmetric dissociation energy curves for ThO_2 (with $\measuredangle$ (O–Th–O) = 120 degrees at all distances) are depicted in Figure 4. Around the equilibrium geometry, both methods give similar potential energy surfaces but differ for Th–O distances larger than 2.50 Å. While CAS(12,12)SCF shows no shoulder region, AP1roG predicts a plateau in the potential energy surface, similar to UO_2^{2+}. We should emphasize that the Th–O bond dissociates at a much longer distance than the U–O bond in UO_2^{2+} (4.50 Å vs. 3.30 Å, respectively).

An in depth analysis of the AP1roG wave function at different Th–O bond lengths is presented in Figure 5. Around the equilibrium distance, the ThO_2 wave function is well-represented by a single electron configuration (see Figure 5a), where the most important orbitals are the π-type orbitals (22,23) between thorium and oxygen and localized p-orbitals (20,21) on the oxygen atoms. If the Th–O bond is stretched, the π-type orbitals become strongly entangled and reach the maximum value of $s(1)_i$ around the shoulder region (approximately 2.5 Å, see Figure 5c). Beyond this point, the localized oxygen p orbitals interact with thorium d orbitals (20,21,26,27). For increasing Th–O distances, the single-orbital entropy of the d orbitals (20,21,26,27) increases gradually (see Figures 5d–5f). In the vicinity of dissociation, 8 singly occupied orbitals are maximally entangled suggesting a [Rn]: $6d^2 7s^2$ electronic configuration.

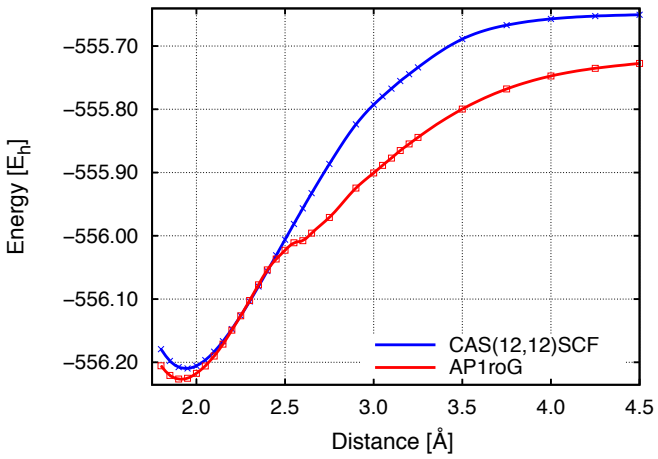

Fig. 4 AP1roG and CASSCF potential energy surfaces for the symmetric dissociation of ThO_2. The O–Th–O angle was kept frozen at 120 degrees during the dissociation process.

3.2 Energetic Stability of ThC_2 Isomers

Actinide carbides form a novel type of nuclear fuel that can be used in Generation IV nuclear power plants.[107] Recent quantum chemical studies on uranium and thorium carbides (UC_n and ThC_n, where $n = 1 - 6$) highlight their complex electronic structure.[107,122,123] Specifically, many different uranium and thorium carbide structures are close in energy, and multi-reference methods are required to correctly predict their relative stability.[107]

In this work, we investigate the energetic stability of ThC_2 compounds in three structural arrangements as shown in Figure 1. All three actinide species have singlet ground states. Total energies for **1**, **2**, and **3** obtained from HF, MP2, AP1roG, and CAS(10,14)SCF are collected in Table 3. Consistent with our previous observations made for systems composed of main group elements only,[92] AP1roG total energies are lower than those calculated from CAS(10,14)SCF (approximately 25 mE_h for **1** and **2**, approximately 15 mE_h for **3**).

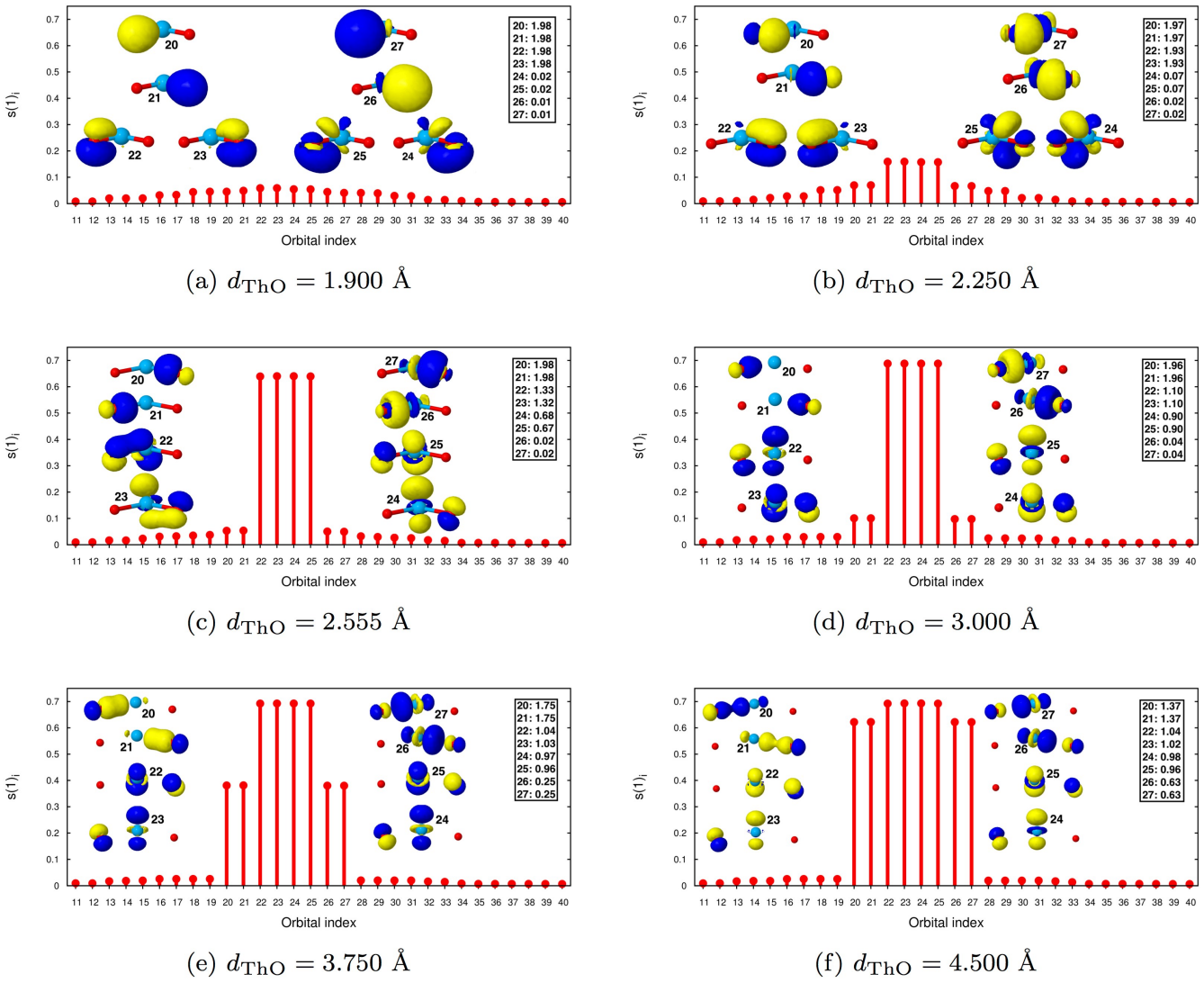

(a) $d_{\mathrm{ThO}} = 1.900$ Å (b) $d_{\mathrm{ThO}} = 2.250$ Å

(c) $d_{\mathrm{ThO}} = 2.555$ Å (d) $d_{\mathrm{ThO}} = 3.000$ Å

(e) $d_{\mathrm{ThO}} = 3.750$ Å (f) $d_{\mathrm{ThO}} = 4.500$ Å

Fig. 5 Comparison of AP1roG single-orbital entropies $s(1)_i$, valence orbitals, and their natural occupation numbers for the ThO_2 molecule at different inter-atomic distances. $s(1)_i$ and the natural occupation numbers are determined from the response 1-RDM.

Table 3 Comparison of total and relative energies of the ThC_2 compounds[a].

Method	Total Energy [E_h]			ΔE [kcal/mol]		Dipole moment y/z [D]		
	1	**2**	**3**	Δ_{12}	Δ_{13}	**1**	**2**	**3**
HF	−481.726 985	−481.729 800	−481.482 422	−1.8	153.5	0.00/4.82	−1.40/5.53	0.00/6.70
AP1roG	−481.937 655	−481.937 049	−481.725 604	0.4	133.1	0.00/5.03	−1.34/5.30	0.00/8.84
CAS(10,14)SCF	−481.912 039	−481.912 180	−481.711 247	−0.1	126.0	0.00/4.05	−0.03/5.17	0.00/7.62
MP2	−482.828 594	−482.829 503	−482.577 139	0.6	157.8	0.00/4.76	−1.63/5.56	0.00/5.48
CASPT2[b]				2.1	118.7			

[a] Δ_{12} and Δ_{13} denote energy difference between structures **1** and **2**, and structures **1** and **3**, respectively.
[b] Ref. 107

All methods studied in this work predict a rather small energy difference (Δ_{12}) between **1** and **2** of at most 2 kcal/mol, suggesting that **1** and **2** are equi-energetic. Furthermore, the z-component of the dipole moment is similar for **1** and **2** (around 5D, see Table 3).

We should emphasize that a perturbative treatment of dynamic correlation on top of CASSCF (CASPT2) increases Δ_{12} from -0.1 kcal/mol to 2.1 kcal/mol.

Stabilization energies for **3** with respect to **1** (Δ_{13}) strongly depend on the electronic structure method, with differences as large as 35 kcal/mol. While AP1roG, CASSCF, and CASPT2 predict the smallest Δ_{13} of about 120–130 kcal/mol, HF, and MP2 yield much larger energy splitting of approximately 150–160 kcal/mol. Large discrepancies between HF and MP2 compared with other correlated approaches can be explained by the strong multi-reference character of **3** (*vide infra*), which is poorly described in HF and MP2 theory. One should also note that HF and MP2 yield the smallest dipole moment for **3** (cf. Table 3).

The CAS(10,14)SCF wave function indicates that **1** and **2** have a single-reference nature (large CI expansion coefficients of the principle configuration of 0.94 and 0.90, respectively), while for **3** several determinants are important with a CI expansion coefficient of 0.76 for the principle configuration. Moreover, the MP2 natural occupation numbers deviate significantly from AP1roG and CAS(10,14)SCF natural occupation numbers (see Figure 6) for **3**. Specifically, only AP1roG and CAS(10,14)SCF yield orbitals with natural occupation numbers close to 0.5 and 1.5, indicating the inappropriateness of MP2.

Figure 7 presents the valence optimized orbitals obtained from the AP1roG wave function and their natural occupation numbers. **1** and **2** have similar natural orbitals that are strongly localized and possess almost identical contributions from atomic orbitals. These orbitals resemble very well the characteristic CASSCF orbitals reported by Pogány *et al.*,[107] with the only difference being that the carbon σ and π molecular orbitals in AP1roG are localized (symmetry-broken). In contrast to **1** and **2**, the valence natural orbitals of **3** are more delocalized and have different atomic contributions from **1** and **2** (cf. Figure 7).

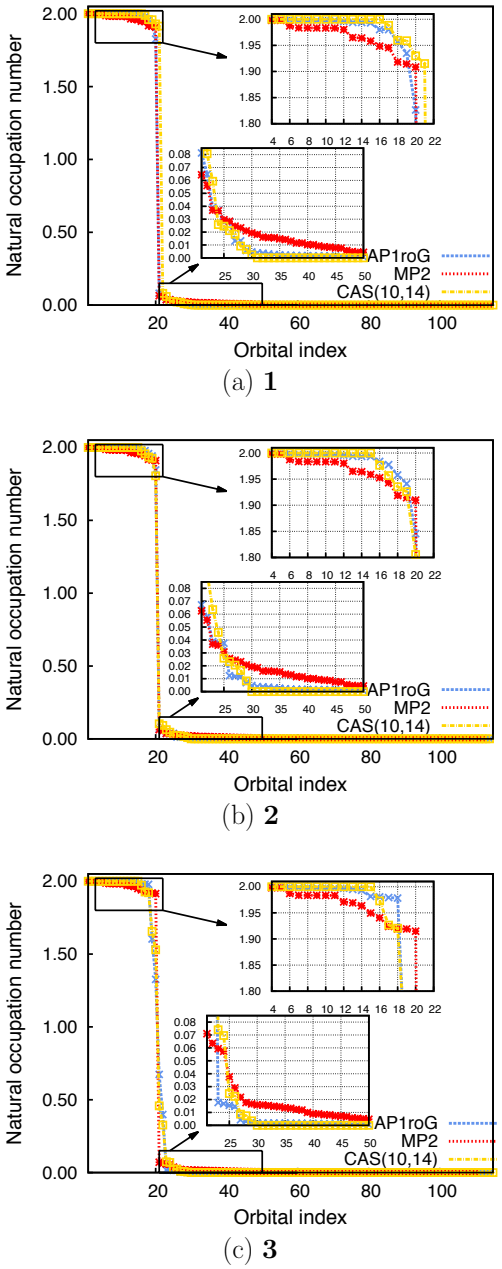

Fig. 6 Analysis of natural occupation numbers for the ThC_2 molecule. The natural occupation numbers are determined from the response 1-RDM and sorted in descending order.

4 Conclusions and Outlook

In this work, we presented the first application of the AP1roG method to actinide chemistry. Our study demonstrates that AP1roG provides qualitatively correct potential energy surfaces for the dissociation of UO_2^{2+} and ThO_2, while conventional methods fail. AP1roG spectroscopic constants (bond lengths and symmetric stretching vibrational frequencies) of UO_2^{2+} and ThO_2 are in good agreement with CCSD(T), the gold standard of quantum chemistry. Our study further suggests that 12-orbital active spaces are unbalanced active spaces in CASSCF calculations when the U–O bonds are stretched.

Furthermore, we showed that AP1roG reproduces CASSCF/CASPT2 stabilization energies for the structural isomers of ThC_2. Specifically, AP1roG correctly predicts that **1** and **2** are equi-energetic, while the distribution of

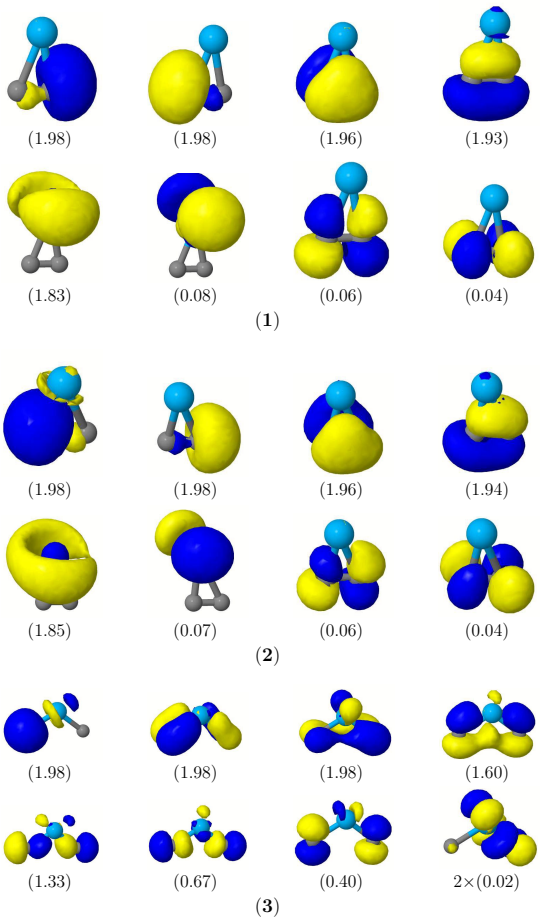

Fig. 7 Comparison of valence AP1roG orbitals and their occupation numbers for ThC_2 species (structures **1**–**3**). The natural occupation numbers are determined from the response 1-RDM. 2× indicates the presence of another orbital (mirror plane) with the same natural occupation number.

natural occupation numbers indicates that **3** has strong multi-reference character. However, it is difficult to assess which method (CASSCF, CASPT2, and AP1roG) provides more accurate energetics for ThC_2 because highly accurate reference data is missing.

Our first study on small actinide complexes illustrates the good performance of AP1roG for describing the electronic structure of (closed-shell) actinide compounds and motivates computational studies on larger, more realistic actinide-containing materials. Due to its cheap computational cost, AP1roG can be easily applied to larger molecular systems.

While AP1roG provides a reliable, cheap, and robust alternative to the strong electron correlation problem in actinide chemistry, the inclusion of dynamic electron correlation is indispensable in reaching spectroscopic accuracy. Different ways to add dynamical correlation to AP1roG calculations are presently being investigated in our laboratory,[124] as well as the laboratory of Gustavo Scuseria.

5 Acknowledgements

We gratefully acknowledge financial support from the Natural Sciences and Engineering Research Council of Canada. K.B. acknowledges the financial support from the Swiss National Science Foundation (P2EZP2 148650) and the Banting Postdoctoral Fellowship program.

The authors acknowledge support for computational resources from SHARCNET, a partner consortium in the Compute Canada national HPC platform.

References

1 G. J. Hutchings, C. S. Heneghan, I. D. Hudson and S. H. Taylor, *Nature*, 1996, **384**, 341–343.
2 J. Li, B. E. Bursten, B. Liang and L. Andrews, *Science*, 2002, **295**, 2242–2245.
3 I. Castro-Rodriguez, H. Nakai, L. N. Zakharov, A. L. Rheingold and K. Meyer, *Science*, 2004, **305**, 1757–1759.
4 S. C. Bart and K. Meyer, *Struc. Bond.*, 2008, **127**, 119–176.
5 A. R. Fox, S. C. Bart, K. Meyer and C. C. Cummins, *Nature*, 2008, **455**, 341–349.
6 P. L. Arnold, *Nat. Chem.*, 2009, **1**, 29–30.
7 R. J. Baker, *Chem. Eur. J.*, 2012, **18**, 16258–16271.
8 T. W. Hayton, *Nat. Chem.*, 2013, **5**, 451–452.
9 D. M. King, F. Tuna, E. J. L. McInnes, J. McMaster, W. Lewis, A. J. Blake and S. T. Liddle, *Nat. Chem.*, 2013, **5**, 482–488.
10 K. Nash, *Solvent Extr. Ion Exch.*, 1993, **11**, 729–768.
11 K. L. Nash, R. E. Barrans, R. Chiarizia, M. L. Dietz, M. Jensen, P. Rickert, B. A. Moyer, P. V. Bonnesen, J. C. Bryan and R. A. Sachleben, *Solvent Extr. Ion Exch.*, 2000, **18**, 605–631.
12 E. P. Horwitz, D. G. Kalina, H. Diamond, G. F. Vandegrift and W. W. Schulz, *Solvent Extr. Ion Exch.*, 1985, **3**, 75–109.
13 M. Pepper and B. E. Bursten, *Chem. Rev.*, 1991, **91**, 719–741.
14 G. Schreckenbach and G. A. Shamov, *Acc. Chem. Res.*, 2010, **43**, 19–29.
15 K. G. Dyall and J. K. Fægri, *Introduction to Relativistic Quantum Chemistry*, Oxford, New York, 2007.
16 M. Reiher and A. Wolf, *Relativistic Quantum Chemistry.*

The Fundamental Theory of Molecular Science, Wiley, Dordrecht, 2009.
17 T. Fleig, *Chem. Phys.*, 2011, **395**, 2–15.
18 J. Autschbach, *J. Chem. Phys.*, 2012, **136**, 150902.
19 R. G. Denning, *J. Phys. Chem. A*, 2007, **111**, 4125–4143.
20 F. Réal, A. S. P. Gomes, L. Visscher, V. Vallet and E. Eliav, *J. Phys. Chem. A*, 2009, **113**, 12504–12511.
21 P. Tecmer, A. S. P. Gomes, S. Knecht and L. Visscher, *J. Chem. Phys.*, 2014, **141**, 041107.
22 R. J. Bartlett and J. F. Stanton, *Rev. Comput. Chem.*, 1994, **5**, 65–169.
23 K. Boguslawski, P. Tecmer, Ö. Legeza and M. Reiher, *J. Phys. Chem. Lett.*, 2012, **3**, 3129–3135.
24 B. Roos and P. R. Taylor, *Chem. Phys.*, 1980, **48**, 157–173.
25 P. E. M. Siegbahn, J. Almlöf, A. Heiberg and B. O. Roos, *J. Chem. Phys.*, 1981, **74**, 2384–2396.
26 R. J. Buenker, S. D. Peyerimhoff and W. Butscher, *Mol. Phys.*, 1978, **35**, 771–791.
27 B. Jeziorski, *Mol. Phys.*, 2010, **108**, 3043–3054.
28 D. I. Lyakh, M. Musiał, V. F. Lotrich and R. J. Bartlett, *Chem. Rev.*, 2012, **112**, 182–243.
29 A. Landau, E. Eliav, Y. Ishikawa and U. Kaldor, *J. Chem. Phys.*, 2001, **115**, 6862–6866.
30 S. Matsika, Z. Zhang, S. R. Brozell, J.-P. Blaudeau, Q. Wang and R. M. Pitzer, *J. Phys. Chem. A*, 2001, **105**, 3825–3828.
31 K. Pierloot and E. van Besien, *J. Phys. Chem.*, 2005, **123**, 204309.
32 L. Gagliardi and B. Roos, *Nature*, 2005, **433**, 848–851.
33 I. Infante, A. S. P. Gomes and L. Visscher, *J. Chem. Phys.*, 2006, **125**, 074301.
34 I. Infante, M. Vilkas, I. Ishikawa, U. Kaldor and L. Visscher, *J. Chem. Phys.*, 2007, **127**, 124308.
35 F. Réal, V. Vallet, C. Marian and U. Wahlgren, *J. Phys. Chem.*, 2007, **127**, 214302.
36 L. Gagliardi and B. O. Roos, *Chem. Soc. Rev.*, 2007, **36**, 893–903.
37 A. S. P. Gomes, C. R. Jacob and L. Visscher, *Phys. Chem. Chem. Phys.*, 2008, **10**, 5353–5362.
38 T. Yang, R. Tyagi, Z. Zhang and R. M. Pitzer, *Mol. Phys.*, 2009, **107**, 1193–1195.
39 P. Tecmer, A. S. P. Gomes, U. Ekström and L. Visscher, *Phys. Chem. Chem. Phys.*, 2011, **13**, 6249–6259.
40 P. Tecmer, H. van Lingen, A. S. P. Gomes and L. Visscher, *J. Chem. Phys.*, 2012, **137**, 084308.
41 H.-S. Hu, Y.-H. Qiu, X.-G. Xiong, W. H. E. Schwarz and J. Li, *Chem. Sci.*, 2012, **3**, 2786–2796.
42 A. S. P. Gomes, C. R. Jacob, F. Réal, L. Visscher and V. Vallet, *Phys. Chem. Chem. Phys.*, 2013, **15**, 15153–15162.
43 S. Cotton, *Lanthanide and actinde chemistry*, Wiley, Chichester, 2005.
44 P. Tecmer, K. Boguslawski, Ö. Legeza and M. Reiher, *Phys. Chem. Chem. Phys*, 2014, **16**, 719–727.
45 S. R. White, *Phys. Rev. Lett.*, 1992, **69**, 2863–2866.
46 S. R. White, *Phys. Rev. B*, 1993, **48**, 10345–10356.
47 R. G. Parr and W. Yang, *Density Functional Theory of atoms and molecules*, Oxford, New York, 1989.
48 D. Wang, W. F. van Gunsteren and Z. Chai, *Chem. Soc. Rev.*, 2012, **41**, 5836–5865.
49 X.-D. Wen, R. L. Martin, T. M. Henderson and G. E. Scuseria, *Chem. Rev.*, 2013, **113**, 1063–1096.
50 P. F. Souter, G. P. Kushto, L. Andrews and M. Neurock, *J. Am. Chem. Soc.*, 1997, **7863**, 1682–1687.
51 N. Kaltsoyannis, *Inorg. Chem.*, 2000, **39**, 6009–6017.
52 C. Clavaguéra-Sarrio, N. Ismail, C. J. Marsden, D. Bégue and C. Pouchan, *Chem. Phys.*, 2004, **302**, 1–11.
53 G. A. Shamov and G. Schreckenbach, *J. Am. Chem. Soc.*, 2008, **130**, 13735–13744.
54 G. Nocton, P. Horeglad, V. Vetere, J. Pécaut, L. Dubois, P. Maldivi, N. M. Edelstein and M. Mazzanti, *J. Am. Chem. Soc.*, 2009, **132**, 495–508.
55 G. S. Groenewold, M. J. Van Stipdonk, W. A. De Jong, J. Oomens, G. L. Gresham, M. E. McIlwain, D. Gao, B. Siboulet, L. Visscher, M. Kullman and N. Polfer, *ChemPhysChem*, 2008, **9**, 1278–1285.
56 F. Réal, U. Wahlgren and I. Grenthe, *J. Am. Chem. Soc.*, 2008, **130**, 11742–11751.
57 S. Tsushima, *Dalton Trans.*, 2011, **40**, 6732–6737.
58 G. S. Groenewold, M. J. van Stipdonk, J. Oomens, W. A. De Jong, G. L. Gresham and M. E. McIlwain, *Int. J. Mass Spectrom.*, 2010, **297**, 67–75.
59 P. L. Arnold, G. M. Jones, S. O. Odoh, G. Schreckenbach, N. Magnani and J. B. Love, *Nat. Chem.*, 2012, **4**, 221–227.
60 V. Vallet, U. Wahlgren and I. Grenthe, *J. Phys. Chem. A*, 2012, **115**, 12373–12380.
61 P. Tecmer, R. Bast, K. Ruud and L. Visscher, *J. Phys. Chem. A*, 2012, **116**, 7397–7404.
62 P. Tecmer, N. Govind, K. Kowalski, W. A. De Jong and L. Visscher, *J. Chem. Phys*, 2013, **139**, 034301.
63 C. Clavaguéra-Sarrio, V. Vallet, D. Maynau and C. J. Marsden, *J. Phys. Chem.*, 2004, **121**, 5312–5321.
64 F. Gendron, D. Páez-Hernández, F.-P. Notter, B. Pritchard, H. Bolvin and J. Autschbach, *Chem. Eur. J.*, 2014, **20**, 7994–8011.
65 P. A. Johnson, P. W. Ayers, P. A. Limacher, S. De Baerdemacker, D. Van Neck and P. Bultinck, *Comput. Chem. Theory*, 2013, **1003**, 101–113.

66 P. A. Limacher, P. W. Ayers, P. A. Johnson, S. De Baerdemacker, D. Van Neck and P. Bultinck, *J. Chem. Theory Comput.*, 2013, **9**, 1394–1401.

67 K. Boguslawski, P. Tecmer, P. W. Ayers, P. Bultinck, S. De Baerdemacker and D. Van Neck, *Phys. Rev. B*, 2014, **89**, 201106(R).

68 A. C. Hurley, J. Lennard-Jones and J. A. Pople, *Proc. R. Soc. London Ser. A*, 1953, **220**, 446–455.

69 W. A. Goddard and A. Amos, *Chem. Phys. Lett.*, 1972, **13**, 30–35.

70 W. A. Goddard, T. H. Dunning Jr., W. J. Hunt and P. J. Hay, *Acc. Chem. Res.*, 1973, **6**, 368–376.

71 R. G. Parr, F. O. Ellison and P. G. Lykos, *J. Chem. Phys.*, 1956, **24**, 1106–1107.

72 J. M. Parks and R. G. Parr, *J. Chem. Phys.*, 1958, **28**, 335–345.

73 W. Kutzelnigg, *J. Chem. Phys.*, 1964, **40**, 3640–2647.

74 W. Kutzelnigg, *Theoret. Chim. Acta*, 1965, **3**, 241–253.

75 V. A. Rassolov, *J. Chem. Phys.*, 2002, **117**, 5978–5987.

76 A. J. Coleman, *J. Math. Phys.*, 1965, **6**, 1425–1431.

77 S. Bratoz and P. Durand, *J. Chem. Phys.*, 1965, **43**, 2670–2679.

78 D. M. Silver, *J. Chem. Phys.*, 1969, **50**, 5108–5116.

79 D. M. Silver, *J. Chem. Phys.*, 1970, **52**, 299–303.

80 G. Náray-Szabó, *J. Chem. Phys.*, 1973, **58**, 1775–1776.

81 G. Náray-Szabó, *Int. J. Qunatum Chem.*, 1975, **9**, 9–21.

82 P. R. Surján, *Phys. Rev. A*, 1984, **30**, 43–50.

83 P. R. Surján, *Phys. Rev. A*, 1985, **32**, 748–755.

84 P. R. Surján, *Int. J. Quantum Chem.*, 1994, **52**, 563–574.

85 P. R. Surján, *Int. J. Quantum Chem.*, 1995, **55**, 109–116.

86 E. Rosta and P. R. Surján, *Int. J. Quantum Chem.*, 2000, **80**, 96–104.

87 P. R. Surján, in *Correlation And Localization*, Springer, Berlin, 1999, pp. 63–88.

88 E. Rosta and P. R. Surján, *J. Chem. Phys.*, 2002, **116**, 878–889.

89 P. R. Surján, A. Szabados, P. Jeszenszki and T. Zoboki, *J. Math. Chem.*, 2012, **50**, 534–551.

90 P. Tecmer, K. Boguslawski, P. A. Limacher, P. A. Johnson, M. Chan, T. Verstraelen and P. W. Ayers, *J. Phys. Chem. A*, 2014, **118**, 9058–9068.

91 K. Boguslawski, P. Tecmer, P. A. Limacher, P. A. Johnson, P. W. Ayers, P. Bultinck, S. De Baerdemacker and D. Van Neck, *J. Chem. Phys.*, 2014, **140**, 214114.

92 K. Boguslawski, P. Tecmer, P. W. Ayers, P. Bultinck, S. De Baerdemacker and D. Van Neck, *J. Chem. Theory Comput.*, 2014, **10**, 4873–4882.

93 T. M. Henderson, J. Dukelsky, G. E. Scuseria, A. Signoracci and T. Duguet, *Phys. Rev. C*, 2014, **89**, 054305.

94 T. Stein, T. M. Henderson and G. E. Scuseria, *J. Chem. Phys.*, 2014, **140**, 214113.

95 T. M. Henderson, I. W. Bulik, T. Stein and G. E. Scuseria, *J. Chem. Phys.*, 2014, **141**, 244104.

96 P. A. Limacher, T. D. Kim, P. W. Ayers, P. A. Johnson, S. De Baerdemacker, D. Van Neck and P. Bultinck, *Mol. Phys.*, 2014, 853–862.

97 T. Helgaker, P. Jørgensen and J. Olsen, *Molecular Electronic-Structure Theory*, Wiley, New York, 2000.

98 M. Dolg and X. Cao, *Chem. Rev.*, 2012, **112**, 403–480.

99 W. Küchle, M. Dolg, H. Stoll and H. Preuss, *J. Chem. Phys.*, 1994, **100**, 7535–7542.

100 T. H. Dunning, *J. Chem. Phys.*, 1989, **90**, 1007–1023.

101 J. A. Coxon, *J. Mol. Spectrosc.*, 1992, **282**, 274–282.

102 M. Abramowitz and I. A. Stegun, *Handbook Of Mathematical Functions With Formulas, Graphs, And Mathematical Tables*, Dover, New York, 1970.

103 Horton, developer version 1.2, written by T. Verstraelen, S. Vandenrbande, M. Chan, F. H. Zadeh, C. Gonzalez, K. Boguslawski, P. Tecmer, P. A. Limacher, A. Malek, Ghent (Belgium) and Hamilton (Canada), 2013 `http://theochem.github.com/horton/` (accessed November 9, 2014).

104 K. Boguslawski and P. Tecmer, *Int. J. Quantum Chem.*, 2014, 10.1002/qua.24832.

105 H.-J. Werner, P. J. Knowles, R. Lindh, F. R. Manby, P. C. M. Schütz, T. Korona, A. Mitrushenkov, G. Rauhut, T. B. Adler, R. D. Amos, A. Bernhardsson, A. Berning, D. L. Cooper, M. J. O. Deegan, A. J. Dobbyn, F. Eckert, E. Goll, C. Hampel, G. Hetzer, T. Hrenar, G. Knizia, C. Köppl, Y. Liu, A. W. Lloyd, R. A. Mata, A. J. May, S. J. McNicholas, W. Meyer, M. E. Mura, A. Nicklass, P. Palmieri, K. Pflüger, R. Pitzer, M. Reiher, U. Schumann, H. Stoll, A. J. Stone, R. Tarroni, T. Thorsteinsson, M. Wang and A. Wolf, *MOLPRO, Version 2010.1, A Package Of* Ab Initio *Programs*, 2012, see http://www.molpro.net.

106 H.-J. Werner, P. J. Knowles, G. Knizia, F. R. Manby and M. Schütz, *WIREs Comput. Mol. Sci.*, 2012, **2**, 242–253.

107 P. Pogány, A. Kovács, Z. Varga, F. M. Bickelhaupt and J. Rudy, *J. Phys. Chem. A*, 2012, **116**, 747–755.

108 K. Aidas, C. Angeli, K. L. Bak, V. Bakken, R. Bast, L. Boman, O. Christiansen, R. Cimiraglia, S. Coriani, P. Dahle and et. al., *WIREs Comput. Mol. Sci.*, 2013, **4**, 269–284.

109 J. P. Perdew, K. Burke and M. Ernzerhof, *Phys. Rev. Lett.*, 1996, **77**, 3865.

110 M. Ernzerhof and G. Scuseria, *J. Chem. Phys.*, 1999, **110**, 5029.

111 W. A. De Jong, L. Visscher and W. C. Nieuwpoort,

J. Mol. Struct. (Theochem), 1999, **458**, 41.
112 M. Straka, K. G. Dyall and P. Pyykk, *Theor. Chem. Acc.*, 2001, **106**, 393–403.
113 D. Majumdar, K. Balasubramanian and H. Nitsche, *Chem. Phys. Lett.*, 2002, **361**, 143–151.
114 V. E. Jackson, R. Craciun, D. A. Dixon, K. Peterson and W. B. de Jong, *J. Phys. Chem. A*, 2008, **112**, 4095–4099.
115 A. Kovács and R. J. M. Konings, *J. Phys. Chem. A*, 2012, **115**, 6646–6656.
116 K. Tatsumi and R. Hoffmann, *Inorg. Chem.*, 1980, **19**, 2656–2658.
117 K. Dyall, *Mol. Phys.*, 1999, **96**, 511–518.
118 L. Freitag, S. Knecht, S. F. Keller, M. G. Delcey, F. Aquilante, T. B. Pedersen, R. Lindh, M. Reiher and L. Gonzalez, *Phys. Chem. Chem. Phys.*, 2015, –.
119 K. Boguslawski, P. Tecmer, G. Barcza, Ö. Legeza and M. Reiher, *J. Chem. Theory Comput.*, 2013, **9**, 2959–2973.
120 M. Mottet, P. Tecmer, K. Boguslawski, Ö. Legeza and M. Reiher, *Phys. Chem. Chem. Phys.*, 2014, **16**, 8872–8880.
121 C. Duperrouzel, P. Tecmer, K. Boguslawski, G. Barcza, O. Legeza and P. W. Ayers, *Chem. Phys. Lett.*, 2015, **621**, 160–164.
122 S. K. Gupta and K. A. Gingerich, *J. Chem. Phys.*, 1980, **72**, 2795–2800.
123 A. Kovács and R. J. M. Konings, *J. Nucl. Mater.*, 2008, **372**, 391–393.
124 P. Limacher, P. Ayers, P. Johnson, S. De Baerdemacker, D. Van Neck and P. Bultinck, *Phys. Chem. Chem. Phys*, 2014, **16**, 5061–5065.